Research Article

The Role of Changing Loop Conformations in Streptavidin Versions Engineered for High-affinity Binding of the *Strep*-tag II Peptide

Thomas G. M. Schmidt [1], Andreas Eichinger [2], Markus Schneider [2], Lidia Bonet [1], Uwe Carl [1], Dennis Karthaus [1], Ina Theobald [2] and Arne Skerra [2]*

*1 - **IBA GmbH,** Rudolf-Wissell-Str. 28, 37079 Göttingen, Germany*
*2 - **Lehrstuhl für Biologische Chemie,** Technische Universität München, 85354 Freising, Germany*

***Correspondence to Arne Skerra:** skerra@tum.de (A. Skerra)*
https://doi.org/10.1016/j.jmb.2021.166893
Edited by Sachdev Sidhu

Abstract

The affinity system based on the artificial peptide ligand *Strep*-tag® II and engineered tetrameric streptavidin, known as Strep-Tactin®, offers attractive applications for the study of recombinant proteins, from detection and purification to functional immobilization. To further improve binding of the *Strep*-tag II to streptavidin we have subjected two protruding loops that shape its ligand pocket for the peptide – instead of D-biotin recognized by the natural protein – to iterative random mutagenesis. Sequence analyses of hits from functional screening assays revealed several unexpected structural motifs, such as a disulfide bridge at the base of one loop, replacement of the crucial residue Trp120 by Gly and a two-residue deletion in the second loop. The mutant m1-9 (dubbed Strep-Tactin XT) showed strongly enhanced affinity towards the *Strep*-tag II, which was further boosted in case of the bivalent Twin-*Strep*-tag®. Four representative streptavidin mutants were crystallized in complex with the *Strep*-tag II peptide and their X-ray structures were solved at high resolutions. In addition, the crystal structure of the complex between Strep-Tactin XT and the Twin-*Strep*-tag was elucidated, indicating a bivalent mode of binding and explaining the experimentally observed avidity effect. Our study illustrates the structural plasticity of streptavidin as a scaffold for ligand binding and reveals interaction modes that would have been difficult to predict. As result, Strep-Tactin XT offers a convenient reagent for the kinetically stable immobilization of recombinant proteins fused with the Twin-*Strep*-tag. The possibility of reversibly dissociating such complexes simply with D-biotin as a competing ligand enables functional studies in protein science as well as cell biology.

Introduction

Affinity tags offer powerful tools for the generic purification, detection and functional elucidation of diverse recombinant proteins, which are typically associated with a wide range of biochemical and biophysical properties.[1–6] However, depending on the application, the precise requirements for the mode and strength of interaction between the affinity tag and its cognate receptor can vary considerably. For example, column chromatography works best with an intermediate affinity such that high on- and off-rates allow both efficient binding under flow conditions and sharp elution from the affinity matrix by means of a small molecule competitor in a non-denaturing buffer. In contrast, practically useful immobilization on a solid phase requires high affinity with a very slow off-rate to enable subsequent robust assays. Under conditions of column purification, however, such a slow off-rate would require elution under harsh conditions.[7,8]

One obvious solution to these mixed demands is the combination of different affinity tags that provide distinct binding characteristics for various purposes.[2,8] However, the accumulation of multiple tags can significantly affect the properties of the recombinant protein of interest, including unspecific binding or aggregation propensity or diminished enzymatic or ligand-binding activity. Alternatively, the availability of different receptor proteins that cover a spectrum of binding properties for the same short tag offers a more convenient situation. This minimizes modifications to the recombinant protein and reduces the effort when planning the corresponding expression construct.

The development of the *Strep*-tag affinity system started in the 1990s with the random library-assisted discovery of a sequence of 8 proteinogenic amino acids that confer binding activity towards streptavidin – already well established as a biotin-binding protein reagent[9] – if attached to the C-terminus of a recombinant protein of choice.[10] Considering the state at the time, the *Strep*-tag offered two compelling advantages: (i) the commercial availability of streptavidin affinity matrices suitable for chromatographic purification and (ii) the possibility of mild competitive elution with D-biotin, the natural ligand of streptavidin (or using less tightly binding derivatives, for example diaminobiotin), to ensure functional protein recovery.

Subsequent improvements of the technology led to the *Strep*-tag II with a slightly modified peptide sequence, which permitted both N- and C-terminal attachment[11] and, later on, to the Twin-*Strep*-tag, which comprises two *Strep*-tag II motifs in sequential arrangement linked by a 12-residue Gly/Ser spacer.[12] Owing to the avidity effect, which occurs if the bivalent tag simultaneously interacts with two binding sites on the tetrameric streptavidin, the Twin-*Strep*-tag offers the benefit of much tighter binding, in particular lower off-rate, while retaining the fundamental reversibility of the interaction. This allows complex dissociation upon addition of a competitive ligand under the same mild conditions as for the original system.

The initial receptor protein for the *Strep*-tag (II) was the so-called core streptavidin, a commercially available proteolytically truncated version of the secretory biotin-binding protein from *Streptomyces avidinii*, which was later made available as a recombinant protein.[13] The (monovalent) protein-peptide affinity was determined to be in the low double digit micromolar range,[11] which is particularly useful for the efficient affinity purification of multimeric recombinant proteins (exhibiting several copies of the *Strep*-tag). On the other hand, the recovery of monovalent *Strep*-tag fusion proteins from diluted solutions (including cell culture supernatants) was less efficient, thus necessitating high expression levels and elevated density of binding sites on the streptavidin affinity resin.[2,13]

The development of the streptavidin mutants m1 and m2 (available under the trade name Strep-Tactin), in which the flexible loop that reversibly covers the binding site for biotin was engineered to allow tighter binding of the *Strep*-tag II,[14] significantly improved the robustness and application range of the *Strep*-tag system, such that its use rapidly gained popularity.[2–8,15–17] Currently, this system offers affinities from 1 μM, for the *Strep*-tag II, down to 35 nM, for the Twin-*Strep*-tag – if measured for the labelled synthetic peptides, but practically with often even lower dissociation constants (K_D) in the context of fusion proteins. Such low K_D values allow efficient protein purification also from diluted solutions, in particular from cell culture supernatants.[18]

While these reagents already cover a broad range of applications – also complemented by antibodies for the detection of *Strep*-tag fusion proteins in fluorescence microscopy, cytofluorimetry and on western blots[15] – some gaps remained, for example: purification of solubilized membrane proteins expressed at low level in *E. coli*[19] and/or low level of secreted proteins in cell culture supernatant, batch purification using magnetic beads, protein purification under denaturing conditions, and stable protein immobilization on sensor chips combined with optional regeneration.

Consequently, the objective of this study was to improve the affinity between the *Strep*-tag II and Strep-Tactin in a rational/combinatorial protein design approach starting from the previously described streptavidin mutants m1 and m2.[14]

Results

Experimental approach for the guided mutagenesis of streptavidin

Using a similar methodological approach as applied in the preceding study that led to the identification of the first streptavidin mutants with improved *Strep*-tag II binding, m1 and m2,[14] we randomized additional amino acid positions and screened for new mutants with even better binding activity. To this end, we applied site-directed saturation mutagenesis using the polymerase chain reaction (PCR) with degenerate oligodeoxynucleotides as well as a previously developed *E. coli* periplasmic secretion system for functional tetrameric streptavidin via fusion with the OmpA signal peptide in combination with a filter sandwich colony screening assay.[14] In this assay, the secreted streptavidin mutants were released from individual *E. coli* colonies growing on a hydrophilic membrane and were captured on a hydrophobic second membrane placed underneath. At the end of the expression phase, and after separation of this second membrane, binding activity of the immobilized streptavidin mutants was probed with bacterial alkaline phosphatase (BAP) fused with a C-terminal *Strep*-tag II followed by chromogenic reaction.[14] Guided

by the signal strength and pattern, corresponding colonies were identified on the first (upper) membrane – which had been stored at 4 °C on a fresh agar plate – and subjected to propagation in liquid culture, plasmid preparation as well as sequencing of the corresponding mutated coding regions.

Revisiting the previously optimized streptavidin loop formed by residues 45–52

In the preceding study,[14] residues 44–47 adjacent to the structurally flexible loop 45–52 of core streptavidin, which plays a role both for biotin binding[20] and for complex formation with the *Strep*-tag (II),[21] had been subjected to targeted random mutagenesis (Figure 1). In the complex with the natural ligand D-biotin this loop adopts a closed conformation[20] whereas binding of the larger *Strep*-tag (II) peptide implies an open conformation.[21] Screening for improved *Strep*-tag II binding had revealed 2 mutants, m1 and m2, which both demonstrated increased affinity by one order of magnitude as compared to wild-type core streptavidin (wtSA).[14] Interestingly, X-ray analysis revealed that both mutants exhibited the loop 45–52 in a fixed open conformation while the mutated amino acids did not form direct contacts with the bound peptide ligand.[21] Of note, the two streptavidin mutants carried the same amino acid residues at the random positions 46 and 47 (A and R, respectively; Table 1), suggesting that an optimum had been reached there in the combinatorial screening experiment, whereas the positions 44 and 45 differed (44:V/I; 45: T/G), thus indicating the possibility of further optimization.

Consequently, these positions were revisited in the present study while keeping the previously mutated positions 46 and 47 fixed. In addition, position 52, which structurally interacts with residue 45 when the loop adopts the open conformation, was included in the random mutagenesis in order to sample increased structural variability. As result of the new colony screen performed with this library #1

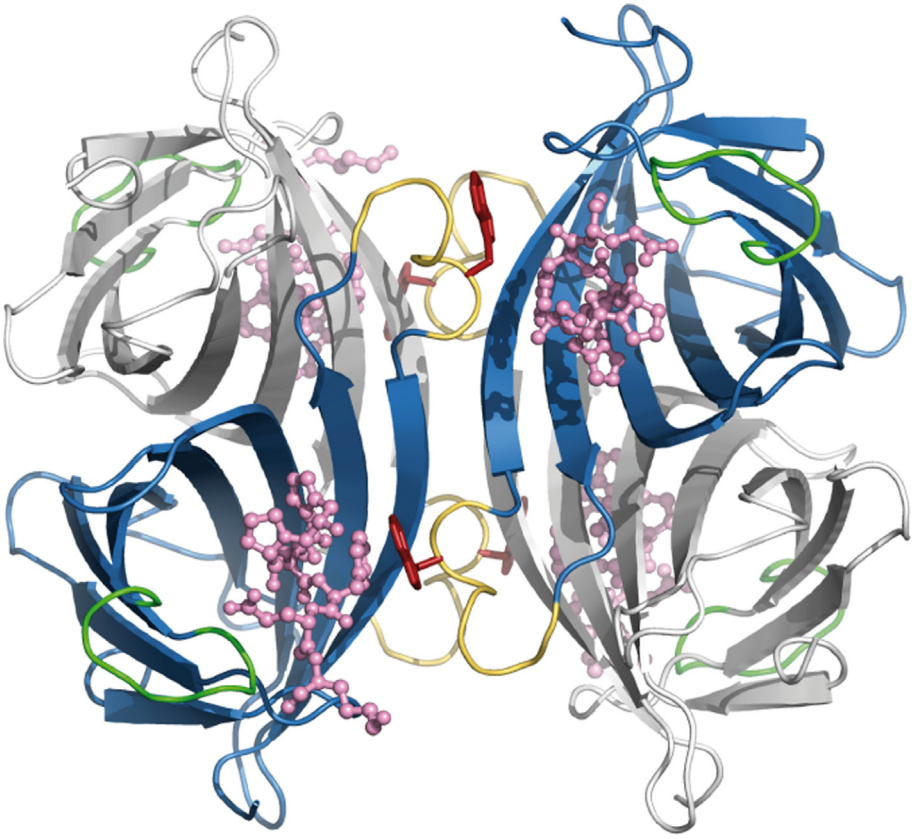

Figure 1. Affinity engineering of *Strep*-Tactin. Crystal structure of the streptavidin mutant m1 tetramer in complex with the *Strep*-tag II (PDB ID: 1KL3). Monomers with their binding sites pointing to the front are shown in blue (chains A and D), those that point to the back are colored gray. The *Strep*-tag II peptide is depicted as ball-and-stick model in pink. The lid-like loop 3/4 (residues 45–52) is highlighted green whereas the loop 7/8 (residues 115–121) on the other side of the ligand is colored yellow. Residue Trp120, which points into the ligand pocket from this loop 7/8 of the opposite subunit, is depicted in red. Note that Trp120 in chain D (front/top) has a different conformation compared to the other three subunits and points away from the *Strep*-tag II, thereby abandoning the π-stacking interaction with Phe8 in the peptide.

Table 1 Optimization of streptavidin by variation of the loop formed by residues 45–52 using the filter sandwich colony screening assay

Streptavidin residues:	44 ... 47... 52		
Wild type sequence:	GluSerAlaVal... Ser		
m1 sequence:	ValThrAlaArg... Ser		
m2 sequence:	IleGlyAlaArg... Ser		
Library (template)	**Random pattern** Prominent hit sequences	**Mutant**	**Signal strength**
#1 (m1)	XaaXaaAlaArg...Xaa		
	IleThrAlaArg...Ser	**m3***	**+**
	GlyCysAlaArg...Cys	**m400**	**++**
	AlaCysAlaArg...Cys	**m402**	**++**
#2 (m1)	A/GCysXaaXaa...Cys		
	AlaCysGlyArg...Cys	**m4001**	**+++**

(approximately 15,000 in total), one mutated streptavidin with pronounced binding activity towards the *Strep*-tag II probe was discovered (dubbed m3*; cf. Table 1) which carried Ile at position 44, like m2, and Thr at position 45, like m1 (see above). This finding suggested that contributions of mutations at the positions 44 and 45 to the recognition of the *Strep*-tag II may be independent of each other.

Interestingly, several other hits in this assay revealed a pair of Cys residues at positions 45 and 52 (see Table 1). These positions flank the flexible loop segment, which indicates formation of an intramolecular disulfide bond that may stabilize its conformation. Previous investigation of streptavidin structures with the corresponding loop in open and closed conformations revealed that only the open conformation allows binding of the *Strep*-tag or *Strep*-tag II.[21] Inspection of both conformations indicated that only the open loop structure would position the side chains of Cys45 and Cys52 in a way compatible with disulfide bond formation. Conversely, once a disulfide bridge between residues 45 and 52 were formed, the loop should be locked in the open conformation, thus effecting high affinity complexation of the *Strep*-tag II.

In an attempt to further improve the structure of the streptavidin loop in the context of this putative disulfide bond, the dedicated mutational library #2 was generated. While all 20 amino acids were permitted at each of the positions 46 and 47, only Ala or Gly were allowed at position 44, i.e. those kind of residues which were found in case of the two double-Cys mutants initially identified during the screening of library #1. The best candidate emerging from the subsequent screening assay (m4001) carried Ala at position 44 and Gly at position 46 (cf. Table 1) – compared to Ala46 in wtSA, m1, m2 and all mutants found before. Interestingly, Arg appeared again at position 47 in this mutant, like in m1 and m2. Although m4001 evoked significantly higher signals in comparison to m1 in the filter sandwich assay as well as in ELISA – both employing BAP fused with the *Strep*-tag II as probe (data not shown) – inferior performance was seen in assays when applying the *Strep*-tag II in the context of other fusion partners or in affinity measurements with the synthetic peptide (see below). Thus, in spite of its interesting structural properties this mutant did not offer a general advantage regarding practical applications.

On the other hand, m4001 refolded more efficiently from inclusion bodies than the initial mutants isolated from the library #1, m400 or m402, when produced at preparative scale using a previously established cytoplasmic expression system for core streptavidin.[13] Even though no redox buffer system was applied, free Cys residues were not detectable in the resulting protein preparation using Ellman's reagent (not shown), indicating efficient formation of the disulfide bridge under air oxygen. In order to elucidate its structural role we co-crystallized the streptavidin mutant m4001 with the synthetic *Strep*-tag II peptide (Abz-SAWSHPQFEK-NH_2). The crystal structure in space group $I4_122$, with one monomer per asymmetric unit, was solved from a synchrotron X-ray diffraction set at a resolution of 2.1 Å (Table 2).

The refined X-ray structure of the m4001 tetramer (generated using crystallographic symmetry) appeared highly similar to the one of the streptavidin mutant m1 (PDB ID: 1KL3)[21]; in particular, the *Strep*-tag II appeared well defined in the electron density map (residues Ser4-Lys10), showing a similar conformation (Figure 2). Compared with m1, the mutant m4001 carries 4 mutations, V44A, T45C, A46G and S52C, while the substitution V47R from wtSA is common to both mutants. As expected, the two introduced Cys residues form a disulfide bridge, which was clearly visible in the electron density. Similar to the structure of m1, the loop exhibits an open conformation which provides space to accommodate the *Strep*-tag II peptide.[21]

In fact, the loop has moved slightly away in m4001 from the bound peptide and forms an even wider pocket. While the loop seems to possess

Table 2 X-ray diffraction data and refinement statistics

Variant/peptide	m4001/ single	m302/single	m36/single	m1-9/single	m1-9/twin	m1/twin
Name of SA mutant	ACGR	H–WY	YNAFM	ENAGY	ENAGY	VTAR
PDB ID	6QW4	6QSY	6TIP	6QBB	6SOS	6SOK
Crystallization conditions	0.75 M Li_2SO_4, 0.1 M HEPES/ NaOH pH 7.5	18 % (w/v) PEG 8000, 0.2 M Li_2SO_4, 0.1 M Tris/HCl pH 8.5	1.1 M $(NH_4)_2SO_4$, 100 mM Na-acetate pH 4.5	12.5 % (v/v) PEGMME 550, 10 mM $ZnSO_4$, 0.1 M MES/NaOH pH 6.5	1.3 M $(NH_4)_2SO_4$, 100 mM Na-acetate pH 4.5	1.6 M $(NH_4)_2SO_4$, 100 mM Na-citrate/-phosphate pH 4.2
Crystal Data:						
Space group	$I4_122$	$I4_122$	$P4_222$	$P22_12_1$	$P4_12_12$	$P4_12_12$
Unit cell dimensions a, b, c [Å], a = b = g = 90°	57.2, 57.2, 175.1	57.3, 57.3, 174.8	57.6, 57.6, 181.9	45.6, 64.2, 78.1	101.8, 101.8, 118.7	101.3, 101.3, 118.3
Monomers per asym. unit	1	1	2	2	4	4
Data Collection:						
Wavelength [Å]	0.91841	0.91841	0.91801	0.91841	0.91801	0.91841
Resolution range [Å][a]	36.70–2.10 (2.21–2.10)	27.21–1.70 (1.79–1.70)	60.64–2.10 (2.21–2.10)	45.56–1.52 (1.60–1.52)	77.25–2.20 (2.32–2.20)	76.97–1.96 (2.07–1.96)
I/σ[I][a]	4.8	8.5	1.1	6.2	6.3	9.6
R_{merge} [%][b]	11.7	6.4	15.6	7.6	9.8	6.6
Unique reflections	8934	16,563	18,752	35,992	32,346	44,784
Multiplicity[a]	10.0 (10.3)	9.5 (9.6)	9.2 (8.5)	4.7 (4.7)	11.2 (11.8)	10.0 (10.6)
Completeness[a]	100.0 (100.0)	100.0 (100.0)	99.8 (99.9)	100.0 (99.8)	100.0 (100.0)	99.9 (99.7)
Refinement:						
R_{cryst}/R^b_{free}	20.0/24.0	16.0/17.9	20.0/22.8	16.2/19.0	21.2/24.7	15.1/18.4
Protein atoms	902	912	1835	1790	3631	3697
Ligand atoms	62	113	152	152	273	248
Solvent atoms	57	70	52	228	129	242
Average B-factor [$Å^2$]						
Protein	20.9	17.5	40.9 (chain A)	16.7	29.8	28.6
Ligands	29.8	31.9	60.8 (chain P)	28.2	39.4	57.6
Water	26.9	26.6	39.8	27.7	28.0	31.3
Geometry:						
R.m.s.d. bond lengths, angles [Å, °]	0.013, 1.621	0.013, 1.716	0.009, 1.631	0.011, 1.483	0.007, 1.502	0.018, 2.148
Ramachandran analysis[c]:						
Core, allowed, generously allowed, disallowed [%]	90.1, 9.9, 0.0, 0.0	91.0, 9.0, 0.0, 0.0	86.6, 12.5, 0.9 0.0	93.0, 7.0, 0.0, 0.0	89.6, 10.4, 0.0, 0.0	90.2, 9.6, 0.0, 0.2

[a] Values in parentheses are for the highest resolution shell; [b] R_{merge}, R_{cryst} and R_{free} according to[49,50 and51], respectively; [c] calculated with PROCHECK.[43]

decreased flexibility due to the disulfide bridge, the peptide ligand appears to have a more relaxed conformation with a less dense environment. The largest deviation occurs at residues Gly46 and Arg47, with a shift by 3.0 and 3.6 Å of their Cα-atoms, respectively. The conformation of the C-terminus of the bound *Strep*-tag II is also affected, as residue Lys10 gets directed towards the mutated loop. The terminal carboxylate group of the peptide forms an additional hydrogen bond with the main chain nitrogen of residue Arg47. Like in the mutant m1, Arg84 forms a salt bridge with residue Glu9 of the peptide, yet involving different side chain conformations.

For comparison, in the crystal structure of the complex between wtSA and biotin[20] the loop 45–52 appears like a lid covering the bound ligand and the side chains of the flanking residues Ser45 and Ser52, here both replaced by Cys, point into opposite directions while their Cα positions show a larger distance (Ser45–Ser52: 7.7 Å; Cys45–Cys52: 5.6 Å; see Figure 2(B)). This demonstrates that these two positions form the joint required to close the lid – accompanied by considerable reorientation of side chains – which is no longer possible once the disulfide bond has formed. As result, a similar open conformation as previously seen for the loop in m1 with a different set of mutated resi-

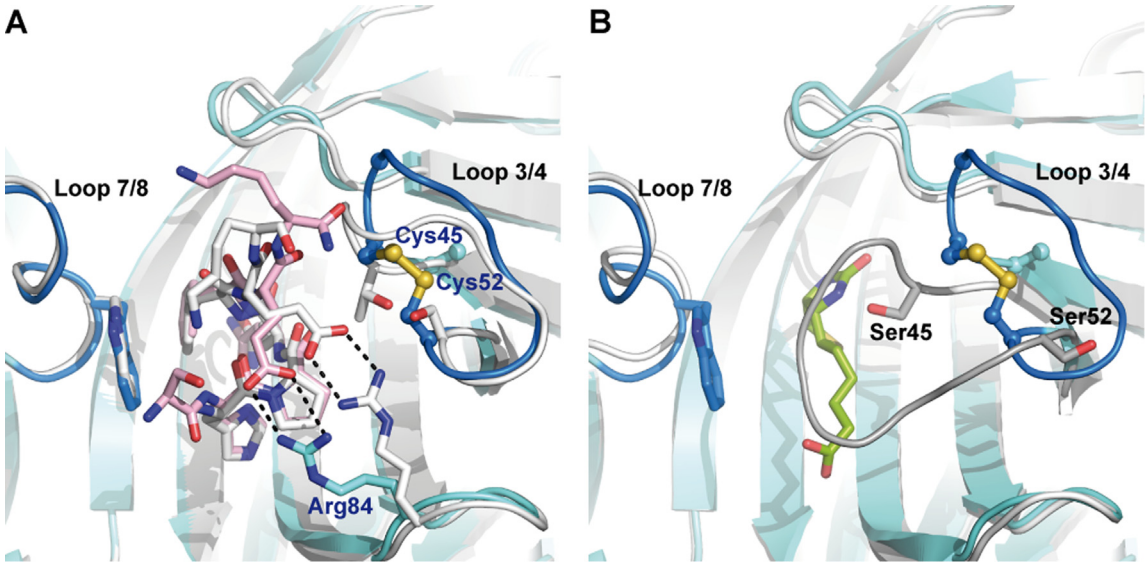

Figure 2. Structural effects of an engineered disulfide bridge in streptavidin. (A) Superimposed crystal structures of the mutants m4001 (light blue) and m1 (light gray; PDB ID: 1KL3), both in complex with the *Strep*-tag II. Loop 3/4 (positions 45–52) in m4001 with the disulfide bridge at its base (marine, sulfur yellow) is seen on the right. Newly mutated side chains in m4001 (Ala44, Cys45, Gly46 and Cys52) are shown as ball-and-sticks; the *Strep*-tag II and the side chain of Arg84 are depicted as stick models, with hydrogen bonds as well as salt bridges indicated as black dotted lines. (B) Superposition of m4001 (*Strep*-tag II omitted) with wtSA (light gray) in complex with biotin (PDB ID: 1STP), using the same coloring as in (A), to illustrate the change in loop conformation. Residues Ser45 and Ser52 in wtSA are shown as sticks and biotin is depicted with carbons in green.

dues is induced by the disulfide crosslink in the streptavidin mutant m4001. Interestingly, loop-stabilizing disulfide bridges have been described for other natural members of the avidin/streptavidin superfamily: in the homo-dimeric rhizavidin, the 3/4 loop is restrained in this manner in a conformation that is competent for biotin binding even in the absence of the 7/8 loop of streptavidin which carries the functionally crucial Trp120 side chain.[22]

Mutagenesis of loop 115–121 in the context of the optimized loop 45–52 of streptavidin

Based on the results so far, the conformation of the loop region comprising residues 44–52 as present in the mutants m1 and m2[14] was considered fully optimized, also in the light of the observation that there were no specific contacts with the bound *Strep*-tag II peptide.[21] Therefore, the crystal structures of m1 and m2, each in complex with the *Strep*-tag II, were examined for other suitable regions to be mutagenized. Our attention was attracted by the side chain of Trp120 in m1, which reaches from the tip of the 115–121 loop into the ligand pocket of the opposite streptavidin subunit on the same face of the tetramer (cf. Figure 1).

As modelled in the published X-ray structure of m1,[21] in 3 of the 4 homo-tetramer subunits the Trp120 side chain adopts a conformation forming a π-stack with residue Phe8 of the *Strep*-tag II whereas in the fourth monomer the indole group appears twisted by 180°, pointing away from the peptide ligand. Furthermore, in both structures of the streptavidin mutants, m1 and m2, the crystallographic B factors of the Trp120 side chain are considerably elevated, indicating structural flexibility and less tight engagement in the complex formation with the *Strep*-tag II, which makes this position a promising target for improvement. Of note, this assessment contrasts with the importance of the same residue for the binding of the natural streptavidin ligand D-biotin. In this case, the affinity drastically drops from 10^{13} M^{-1} to 5×10^{9} M^{-1} or even 8.6×10^{6} M^{-1} upon replacement of Trp120 by Phe or Ala, respectively.[23] Nevertheless, these side chain substitutions are well tolerated by the quaternary structure of streptavidin, rendering this position suitable for mutagenesis in the context of the *Strep*-tag II ligand.

In a first attempt, Trp120 was subjected to random mutagenesis together with positions 117 and 121 in its vicinity (libraries #3 and #4; cf. Table 3). All these side chains are oriented in a way that after appropriate replacements additional contacts with the *Strep*-tag II peptide bound to the opposite streptavidin subunit might be possible. Corresponding random libraries were constructed either in the context of the streptavidin mutant m1 (library #3) or of m4001, which carries the 44–52 loop stabilized in the open conformation in an alternative manner, via a disulfide bridge, as explained above (library #4).

In the filter sandwich screening assay, many colonies with significantly enhanced binding signals were identified for both libraries. Subsequent sequencing of clones with clearly stronger signals compared to m1 revealed 3 different sequence motifs (see Table 3). The most frequent motif was Gly in combination with Tyr or Phe at positions 120 and 121, respectively, typically complemented by a charged or hydrophilic residue at position 117 (predominantly Glu, Gln, Asp or Arg in case of the strongest signals). The second motif carried an aromatic side chain at position 120 (mostly Tyr or Phe, but not Trp) in combination with preferentially small residues at position 121 and complemented by a predominantly bulky hydrophobic residue at position 117. The third motif revealed an unexpected deletion of the two residues 118 and 119, which likely arose from ligation events with PCR products resulting from contaminating truncated oligodeoxynucleotide primers (see Methods). In this case, a Trp residue at position 120 (now 118) in combination with Ala at position 117

Table 3 Optimization of streptavidin by mutating the loop formed by residues 115–121 in combination with the optimized loop 45–52 (from m1 or m4001; cf. Table 1)

Streptavidin residues:	117 ... 121		
Wild type sequence:	AlaAsnAlaTrpLys		
Library (template)	**Random pattern** Prominent hit sequences	**Mutant**	**Signal strength**
#3 (m1)	XaaAsnAlaXaaXaa		
	AspAsnAlaGlyPhe		+++++
	ArgAsnAlaGlyPhe		+++++
	GlnAsnAlaGlyPhe		+++++
	GluAsnAlaGlyPhe		+++++
	TyrAsnAlaGlyPhe	**(Motif 1)**	+++++
	TyrAsnAlaPheMet	**m36**	+++++++
	TyrAsnAlaTyrAla		++++++
	TyrAsnAlaTyrSer		+++++
	PheAsnAlaTyrGly		+++++
	ArgAsnAlaTyrAla		+++++
	TrpAsnAlaTyrGly	**(Motif 2)**	+++++
	Ala------TrpTyr	**m41**	++++++
	Ala------TrpMet	**(Motif 3)**	+++++
#4 (m4001)	XaaAsnAlaXaaXaa		
	GluAsnAlaGlyPhe		++++++
	AspAsnAlaGlyTyr		++++++
	GluAsnAlaGlyTyr	**m9/m1-9**	+++++
	ArgAsnAlaGlyPhe		++++
	ArgAsnAlaMetMet		++++
	GlnAsnAlaMetVal		++++
	AlaAsnAlaMetVal		++++
#5 (m1: refining motif 2)	F/YAsnAlaXaaXaa		
	TyrAsnAlaPheLeu		++++++
	PheAsnAlaPheLeu		++++++
	TyrAsnAlaLeuTrp		++++++
	PheAsnAlaTyrIle		+++++
	TyrAsnAlaTyrLeu		+++++
#6 (m1: refining motif 3)	Xaa------XaaXaa		
	Thr------TrpLeu		++++++
	His------TrpLeu		++++++
	Ile------TrpArg		+++++
	His------TrpThr		+++++
	Thr------TrpArg		+++++
	Ala------TrpArg		+++++
#7 (m1: refining motif 3)	Xaa------TrpXaa		
	Ala------TrpTyr		+++++++
	His------TrpMet		+++++++
	His------TrpTyr	**m302**	+++++++
	Glu------TrpTyr		+++++++
	Gln------TrpTyr		+++++++

and a bulky residue at position 121 appeared to be crucial for increased binding activity.

Based on these findings, the motifs 2 and 3 were further investigated by creating focused libraries in the context of the original mutant m1 (see Table 3). Library #5 was devised to elucidate which amino acid residues at positions 120 and 121 cooperate best with a bulky residue at position 117 (Tyr/Phe) in accordance with motif 2. As result, Tyr or Phe were confirmed as optimal candidates for position 120, accompanied by a bulky aliphatic residue, preferentially Leu, at position 121. Libraries #6 and #7 were constructed to assess the optimal surrounding of motif 3 with the accidentally deleted residues 118 and 119. These deletion events were rare contaminations in the library #3, probably due to a pair of 5′-truncated oligodeoxynucleotide primers (each of the forward and reverse primers, giving rise to PCR products with a ligation site between positions 118 and 119, shortened by 3 nucleotides). Therefore, it was unclear whether the mutated residues arising at positions 117, 120 and 121 constituted an optimal structural arrangement in this context. Based on the screening of library #6, a clear preference for Trp at position 120 (now 118) was established whereas Ala was no longer preferred at position 117 (still noting the absence of bulky hydrophobic residues there). Library #7 was finally generated to further optimize the environment of Trp at the new position 118. As a result, Tyr emerged as preferred residue at the new position 119 while longer hydrophilic side chains predominated at position 117.

In order to gain insight into the mode of improved molecular recognition of the *Strep*-tag II, representative streptavidin mutants for each of the three motifs (all carrying the original sequence of m1 in the 44–52 loop region) were produced at preparative scale and subjected to X-ray crystallographic analysis: m1-9 for motif 1, m36 for motif 2 and m302 for motif 3 (cf. Table 3).

Crystallographic analysis of streptavidin mutants with an engineered loop 115–121

The complex of the streptavidin mutant m1-9 (dubbed *Strep*-Tactin XT) with the *Strep*-tag II peptide crystallized in space group $P22_12_1$ with two monomers per asymmetric unit, and the structure was solved from a synchrotron X-ray data set at 1.5 Å resolution (Table 2). The gross structure of the tetramer (generated via crystallographic symmetry) was similar to the one of m1 with the bound *Strep*-tag II, and the peptide residues Trp3-Lys10 were visible in the electron density with a similar conformation. Despite the three amino acid substitutions of m1-9 in the loop 115–121 compared to m1, A117E, W120G and K121Y (cf. Table 3), its backbone conformation remained unchanged (Figure 3). However, the

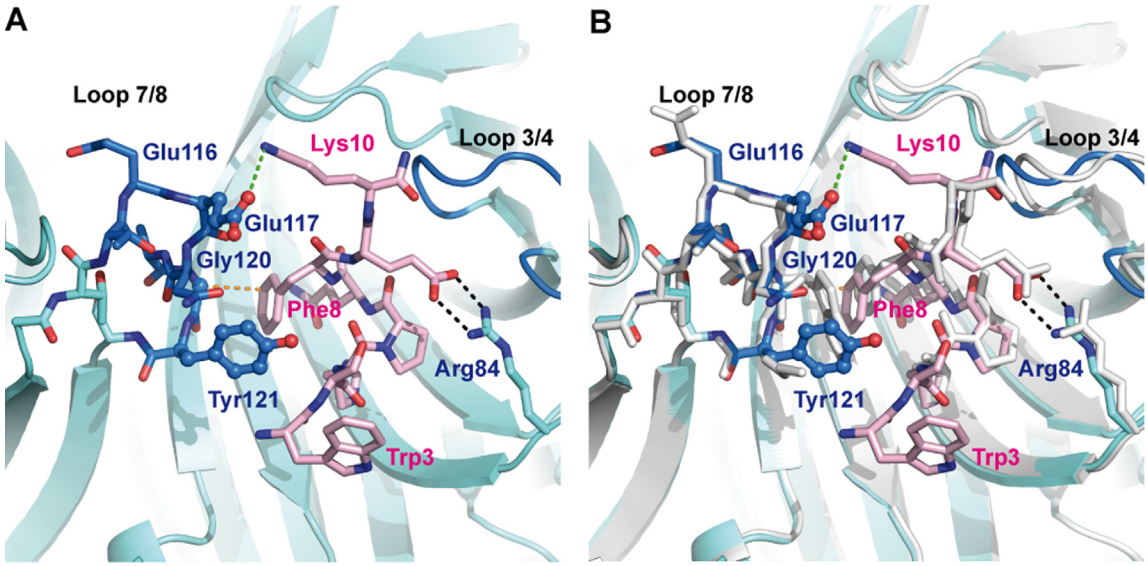

Figure 3. Crystal structure of the streptavidin mutant m1-9. (A) Crystallized complex between m1-9 (light blue) and the *Strep*-tag II (light pink). Mutated side chains are shown as ball-and-sticks. The charged side chain of Arg84 (whose role was already described for the mutant m1)[11] is depicted as stick model and its hydrogen bonds and salt bridge to the peptide residue Glu9 are indicated as black dotted lines. A new salt bridge is formed between the mutated residue Glu117 and the terminal Lys residue of the *Strep*-tag II (green dotted line). Furthermore, the closest distance between the Cα atom of Gly120 (small sphere) and residue Phe8 of the *Strep*-tag II is indicated by a dotted line (orange). Any side chain at this position, if present, would point into the same direction and lead to a clash. (B) Superposition of the streptavidin mutants m1-9 and m1, illustrating a conserved backbone conformation of their 115–121 loops as well as similar orientation of the bound *Strep*-tag II peptide (light gray; PDB ID: 1KL3).

mode of interaction with the *Strep*-tag II – bound to the ligand pocket of the opposite subunit on the same face of the tetramer – showed considerable deviations. In particular, it appears that the Tyr side chain at position 121 has adopted the role of the original residue Trp120, whose side chain is completely missing due to the Gly substitution. In fact, by approaching the *Strep*-tag II from a different angle, the side chain of Tyr121 seems to interact with the peptide in the ligand pocket in a more favorable manner. The side chain of peptide residue Phe8, which previously formed a π-stacking interaction with the Trp120 side chain, now nestles in a hydrophobic niche formed by the Cα methylene group of Gly120 and one face of the aromatic Tyr121 side chain. Moreover, the mutated side chain of Glu117 gives rise to a second salt bridge with peptide residue Lys10, in addition to the one between Arg84 and peptide residue Glu9 (see Figure 3).

The switched role between Trp120 and Tyr121 creates additional space within the ligand pocket and allows a more relaxed conformation of the bound *Strep*-tag II. The closest distance between loop 115–121 and the side chain of peptide residue Phe8 has increased from 3.2 Å in m1 to 3.6 Å in m1-9. It is the substitution W120G which provides the necessary space for residue Tyr121 in its observed new orientation. The lack of a side chain at this position seems crucial for proper interaction with the slightly rearranged peptide ligand whereas an Ala residue would already lead to a clash with the Phe8 phenyl ring. This is supported by the strong conservation of Gly120 in the context of Tyr or Phe at position 121 that was seen after screening of the libraries #3 and #4 (see motif 1 in Table 3).

The complex of the streptavidin mutant m36 with the *Strep*-tag II peptide crystallized in space group $P4_222$, with 2 monomers per asymmetric unit, and its structure was solved from a synchrotron X-ray data set at 2.2 Å resolution (Table 2). Again, the overall structure of the (reconstituted) tetramer was similar to the one of m1 in complex with the *Strep*-tag II while the peptide residues Trp3-Lys10 appeared well defined in the electron density map. Interestingly, in the mutant m36 the backbone conformation of the loop 115–121 that harbors three mutations, A117Y, W120F and K121M (cf. Table 3), is significantly different from the one of m1 (Figure 4). It seems that the substitution of Ala117 by Tyr has led to a conformational change of the entire loop, with a particularly large shift of 6.8 Å between their Cα positions. While Ala117 – in wtSA as well as in the mutant m1 – points away from the streptavidin β-barrel into solvent the side chain of Tyr117 in m36 folds back onto a neighboring subunit, where it contacts the backbone of Thr106, flanked by the side chains of Asn105 and Gln107 on the same β-strand.

As a consequence of this local structural rearrangement, the side chain of the neighboring (unmutated) residue Glu116 can form a new salt bridge with Lys10 in the *Strep*-tag II. In this way, Glu116 adopts the role of the mutated residue Glu117 in the mutant m1-9 described above (cf. Figure 3). Furthermore, the side chain of Phe120, which replaces the original Trp residue in m1, is laterally shifted, now contacting the side chain of His4 in the peptide rather than Phe8, while adopting the preferred conformation that was seen for Trp120 in the three monomers of the previously crystallized complex between m1 and the *Strep*-tag II as described above (cf. Figure 1).

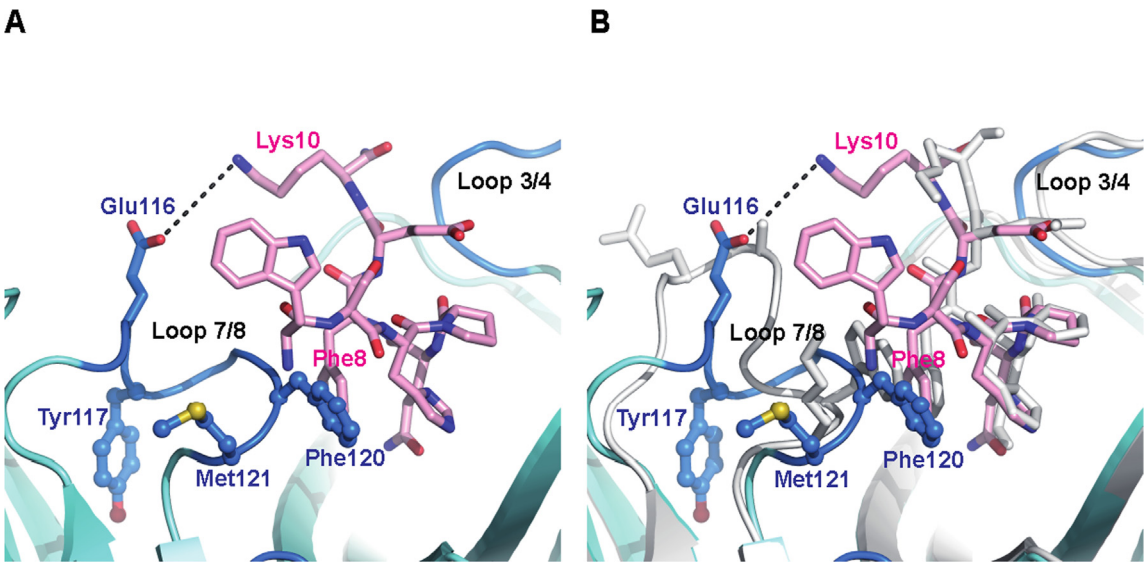

Figure 4. Crystal structure of the streptavidin mutant m36. (A) Crystallized complex between m36 (light blue) and the *Strep*-tag II (light pink). Mutated side chains in streptavidin are shown as ball-and-sticks. (B) Superposition of the streptavidin mutants m36 and m1 (light gray; PDB ID: 1KL3).

Overall, as judged from visual inspection, the binding site is slightly wider and the conformation of the *Strep*-tag II appears more relaxed than in the parental mutant m1 (see Figure 4).

The complex of the streptavidin mutant m302 with the *Strep*-tag II peptide crystallized in space group $I4_122$, with one monomer per asymmetric unit, and the structure was solved from a synchrotron X-ray data set at 1.7 Å resolution (Table 2). Once again, the overall structure of the (reconstituted) tetramer was similar to the one of the streptavidin mutant m1 with the bound *Strep*-tag II. This time, residues Ala2–Lys10 of the *Strep*-tag II were visible in the electron density and the peptide also showed a similar conformation. Notably, the loop 115–121 in m302, with positions 117 and 118 in the streptavidin sequence deleted as explained above, is shorter by two residues than in m1 (see Table 3). In addition, this loop carries two substitutions, A117H and K121Y (according to the numbering of wtSA). Due to the deletion, the backbone conformation of loop 115–121 deviates drastically from the one in m1 and provides significantly more room for the ligand (Figure 5).

The structural differences start at residue Thr114, which shows a flipped peptide bond. More pronounced deviations are evident at residues Thr115 and Glu116, which form a kind of 'shortcut' in the polypeptide backbone of m302 and show displacements of their Cα positions by 4.1 Å and 3.6 Å, respectively, from the corresponding coordinates in m1. Downstream of position 122 the loop turns into β-strand 8 of streptavidin (residues 123–131), then converging again with the structure of m1. Interestingly, the role of Tyr121 resembles the equivalent residue in the streptavidin mutant m1-9 described above: it forms a hydrophobic contact with the side chain of peptide residue Phe8. In this way it replaces the otherwise conserved Trp120 side chain, which is here moved away from the bound peptide as a consequence of the deletion. Like in m1-9, this is accompanied by an increase in the closest distance to the peptide residue Phe8, from 3.2 Å in m1 (Trp120) to 3.6 Å in m302 (Tyr121). Interestingly, residue Trp3 in the *Strep*-tag II is exceptionally well-defined in the electron density – contrasting to all other streptavidin complexes described in this study – and contacts Tyr121 as the nearest residue with a distance of 3.4 Å.

In the shortened loop of streptavidin, residue Trp120, which was found highly conserved in the specialized library #6 (see Table 3), adopts a central position in the middle of a cluster of hydrophobic side chains including the directly neighboring residues Tyr121 and His117 as well as the aliphatic moiety of the Glu116 side chain within the loop, Phe8 from the bound *Strep*-tag II as well as Leu25 from a different loop in the opposite streptavidin subunit (see Figure 5). This arrangement creates more space in the binding site and leads to a more relaxed conformation of the peptide ligand, which is illustrated by the movement of the Phe8 side chain towards the loop as mentioned above. Of note, the side chains of the four adjacent loop residues, Glu116,

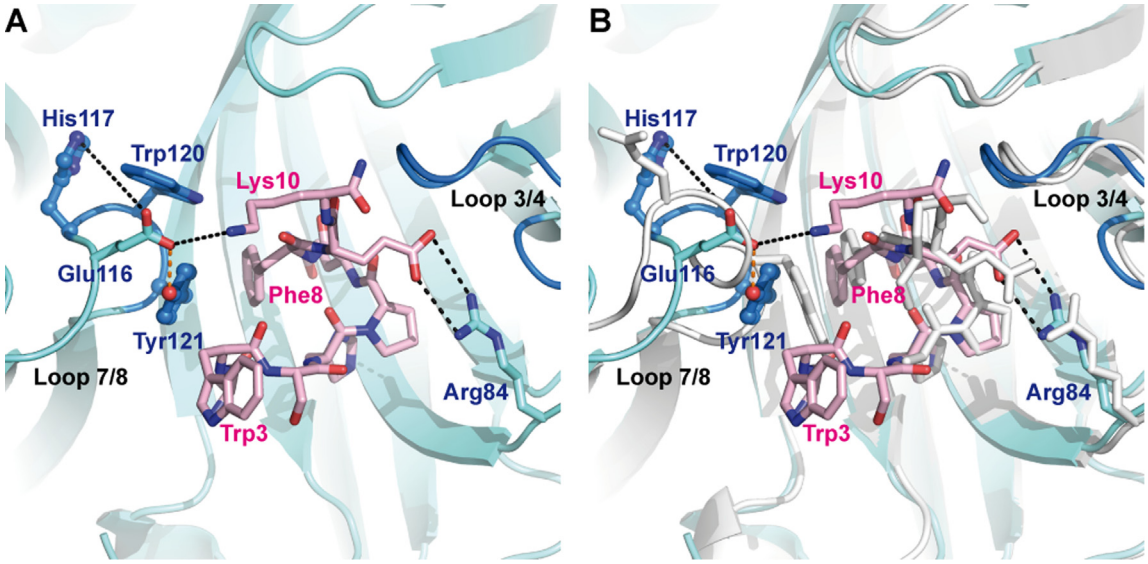

Figure 5. (A) Crystal structure of the streptavidin mutant m302. (A) Crystallized complex between m302 (light blue) and the *Strep*-tag II. Mutated side chains are shown as ball-and-sticks. Glu116 is engaged in a hydrogen bond with Tyr121 (orange dotted line) and can form attractive electrostatic interactions both with Lys10 in the *Strep*-tag II (5.4 Å distance) and, at a larger distance (8.1 Å), with the neighboring His117 side chain. (B) Superposition of the streptavidin mutants m302 and m1 (light gray; Trp120 in the preferred conformation; PDB ID: 1KL3), illustrating the new position of the (unmutated) Glu116 side chain in vicinity to the bound peptide after deletion of two residues, 118 and 119, within the loop 115–121 of streptavidin.

His117, Trp120, Tyr121, all point into the same direction, which is only possible due to the more restrained backbone conformation of the shortened loop 115–121. As a consequence, a hydrogen bond is formed between the Tyr121 hydroxyl group and the Glu116 carboxylate. In this new position, which differs from the one in the parental mutant m1, Glu116 forms both a salt bridge to Lys10 from the *Strep*-tag II and, at a larger distance, to the side chain of His117 within the loop. Thus, it appears that the mutant m302 again provides an alternative structural mechanism to functionalize the unmutated residue Glu116 for improving the interaction with the bound peptide, as similarly seen for m1-9 with the mutated residue Glu117 (His117 in m302).

Complexes of streptavidin mutants with the Twin-*Strep*-tag

The Twin-*Strep*-tag, which comprises 2 *Strep*-tag II sequence motifs arranged in tandem, with a 12 residue Gly/Ser spacer in between,[12] represents a chain of L-amino acids and, thus, does not show rotational C_2 symmetry. Co-crystallisation of this peptide with streptavidin in a way that two binding sites within the homo-tetramer get occupied simultaneously is unlikely in a space group where the corresponding C_2 axis of the tetramer coincides with a crystallographic symmetry axis because the bound peptide would violate the crystallographic symmetry. Unfortunately, wtSA[20] and also many of its mutants crystallize in the space group $I4_122$ (cf. Table 2), where one monomer occupies the asymmetric unit and the biological tetramer results from application of two orthogonal crystallographic C_2 axes, which is incompatible with a doubly bound Twin-*Strep*-tag peptide. Consequently, a search for crystallization conditions of a suitable streptavidin mutant leading to crystals that harbor a complete tetramer in the asymmetric unit was pursued.

We first succeeded in crystallizing the complex of the streptavidin mutant m1 with the synthetic Twin-*Strep*-tag peptide (Abz-SAWSHPQ FEKGGGSGGGSGGSAWSHPQFEK-NH_2) in the presence of ammonium sulfate in the space group $P4_12_12$, with one tetramer in the asymmetric unit. The structure was solved from a synchrotron X-ray data set at 2.0 Å resolution (Table 2). The overall structure of the tetramer was similar to the one of m1 with the bound monomeric *Strep*-tag II, which was previously crystallized in the space group $P2_1$[21] (PDB ID: 1KL3). Residues of the peptide ligand now visible in the electron density (Ser4–Lys10) were the same as in the complex with the plain *Strep*-tag II peptide, whereas residues of the flexible Gly/Ser linker in the Twin-*Strep*-tag were crystallographically not defined. The high similarity of the complex containing the Twin-*Strep*-tag with the one of the monomeric *Strep*-tag II is reflected by the low root mean square deviation (RMSD) calculated after superposition of the streptavidin backbone Cα atoms, resulting in 1.16 Å for the entire streptavidin tetramer.

In a second attempt, the complex of the streptavidin mutant m1-9 with the Twin-*Strep*-tag peptide was also crystallized in the space group $P4_12_12$ with one tetramer in the asymmetric unit, again using ammonium sulfate at a similar pH (see Table 2). The crystal structure was solved from a synchrotron X-ray data set at 2.2 Å resolution. As expected, the overall structure of the streptavidin tetramer was similar to the one of m1 with the bound *Strep*-tag II. Likewise, the *Strep*-tag II residues visible in the electron density (Ser4–Gly12 and Ala22–Lys30) showed a similar conformation. Furthermore, the structure was virtually identical with the one of the mutant m1-9 in complex with the monomeric *Strep*-tag II peptide described above: superposition of all equivalent streptavidin Cα atoms of m1-9/Twin-*Strep*-tag (chain A of the asymmetric unit) with m1-9/*Strep*-tag II (chain A) resulted in an RMSD as low as 0.75 Å.

However, this time electron density (at 1 σ) for the residues Gly11 and Gly12 at the beginning of the linker within the Twin-*Strep*-tag was visible at one binding site of the tetramer (chain A). On the other hand, the *Strep*-tag II sequence beginning with Ala22 at the end of the linker was well defined in the density of the opposite binding site (chain B). Using this structural information for the pair of adjacent streptavidin subunits, we were able to tentatively model the complete Twin-*Strep*-tag peptide with plausible stereochemistry clearly in one of its two possible orientations, thus spanning neighboring binding sites within the streptavidin tetramer (Figure 6).

In contrast, the pair of binding sites on the opposite face of the tetramer revealed defined density only for the two central *Strep*-tag II sequence motifs; hence, it remains unclear which linker connectivity within the Twin-*Strep*-tag is present there – or if the crystal contains a mixture of the two arrangements with a maximally disordered stretch of amino acids in between. Besides, the theoretical possibility of the Twin-*Strep*-tag peptide bridging two streptavidin tetramers within the crystal lattice seems unlikely as the distance between accessible binding sites is too large. Therefore, this crystal structure provides strong indication that the Twin-*Strep*-tag peptide can indeed span two binding sites on one face of the streptavidin homo-tetramer, which explains the remarkable avidity effect observed in corresponding binding experiments (see below) from a structural perspective.

Quantitative binding studies with the new streptavidin mutants

The equilibrium dissociation constants between the purified streptavidin mutants and the *Strep*-tag II peptide, or the Twin-*Strep*-tag, were measured

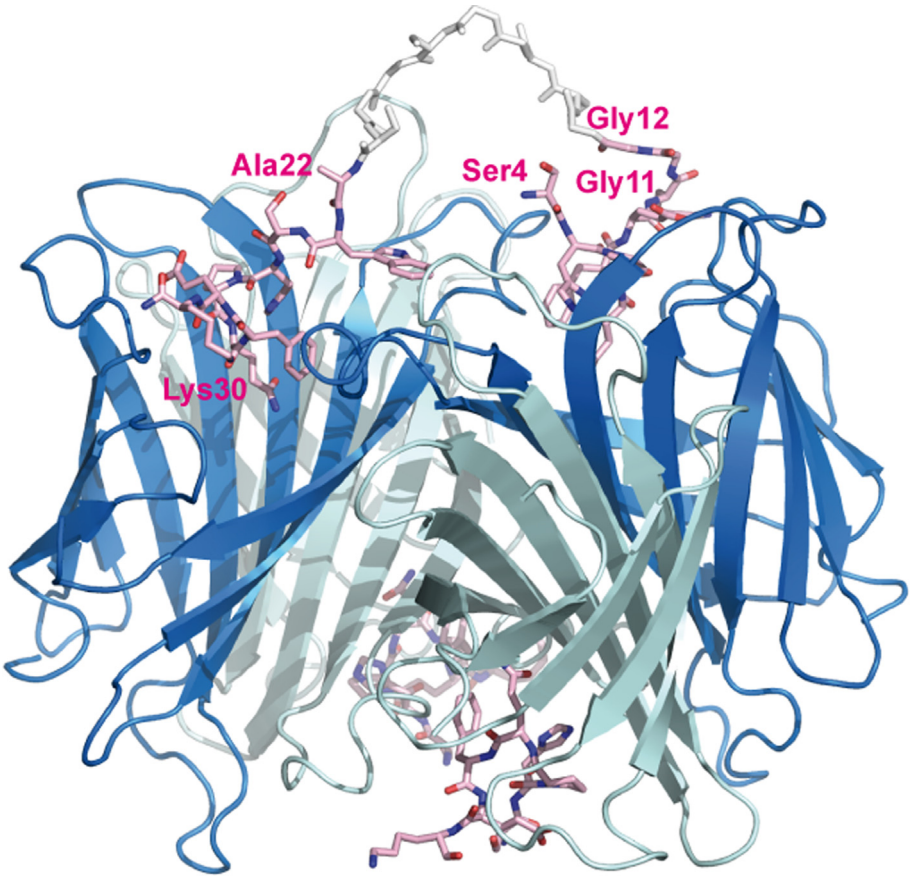

Figure 6. Crystal structure of the streptavidin mutant m1-9 tetramer (Strep-Tactin; subunits shown in shades of blue) in complex with the Twin-*Strep*-tag (light pink, peptide chain P bound to streptavidin chains A and B, shown as stick model). Residues 13–21 comprising the majority of the linker were tentatively modelled in the absence of well defined electron density and are colored gray; residues discussed in the text are labelled.

using a fluorescence titration assay as earlier developed during the engineering of the mutant m1.[14] To this end, both synthetic peptides were equipped with an o-aminobenzoyl (Abz) group at the N-terminus, which undergoes fluorescence resonance energy transfer with the UV-excited Tyr and Trp side chains of the protein and leads to significant fluorescence quenching (at 340 nm) upon complex formation. The dissociation constant (K_D) measured between the mutant m1 and the *Strep*-tag II peptide of 0.39 μM (Table 4) was in the same range as the previously published value (1.4 μM).

The corresponding K_D value for the mutant m4001, which carries a disulfide bridge at the base of the 45–52 loop, was just slightly higher, with 0.6 μM, not quite in agreement with the increased signal intensity that was observed in the filter sandwich colony screening assay. Nonetheless, this confirms that the conformational stabilization of this loop in the open conformation, without involving additional contacts to the ligand, is sufficient to enhance the affinity for the *Strep*-tag II peptide *versus* wtSA, in line with the similar structural effect previously observed for the side chain substitutions at positions 44, 45 and 47 (cf. Table 1) in the mutant 1.[14,21] Obviously, there is a threshold in affinity gain for this structural mechanism of conformational loop freezing – as predicted in a preceding study.[21]

Table 4 Equilibrium affinity measurements between streptavidin mutants and the synthetic *Strep*-tag II peptide via fluorescence titration

SA mutant/peptide	K_D ± SD [nM]
m1/*Strep*-tag II	386 ± 36
m1/Twin-*Strep*-tag II	36.1 ± 3.6
m1-9/*Strep*-tag II	74.6 ± 6.6
m1-9/Twin-*Strep*-tag II	8.6 ± 1.6
m302/*Strep*-tag II	119 ± 16
m36/*Strep*-tag II	104 ± 20
m4001/*Strep*-tag II	604 ± 317

In comparison, significantly lower K_D values were seen for the other three mutants investigated here, which harbor an engineered 115–121 loop (Table 3). While m36 and m302 both showed a 3–4-fold improved affinity over m1, the mutant m1-9 (Strep-Tactin XT) revealed an outstanding affinity in this assay, with $K_D \approx 75$ nM. Interestingly, when

the synthetic Twin-*Strep*-tag was applied in the same fluorescence titration setup, the K_D value further dropped by 9-fold to 8.6 nM. This indicates a strong avidity effect, as it has to be expected if this bivalent peptide simultaneously interacts with two binding sites on one face of the streptavidin tetramer (cf. Figure 6). Of note, a similar relative rise in affinity (by a factor ~10) was seen in the titration of the mutant m1 with the bivalent Twin-*Strep*-tag, which illustrates the biophysical nature of the avidity effect – independent of the individual strength and mechanism of interaction at the binding sites.

To further elucidate the affinity of the mutant m1-9 with regard to practical applications, kinetic studies were performed with *Strep*-tag II fusion proteins using real-time surface plasmon resonance (SPR) measurements (Table 5). While the green fluorescent protein (GFP) served in this assay as a representative monomeric fusion partner for the *Strep*-tag II, the bacterial cytochrome b_{562} was used as an example for a monomeric protein where the C-terminal *Strep*-tag (II) exhibits an atypically low affinity both towards streptavidin and Strep-Tactin.[12,13] Indeed, the same effect was seen here with affinities differing by a factor 56–128 or 18–21, respectively, when these different fusion proteins were investigated as mobile analytes *versus* the immobilized streptavidin mutants m1 or m1-9 (also depending on their density on the sensor chip). Of practical relevance is the observation that cytochrome b_{562}, with its negative impact on the *Strep*-tag/streptavidin interaction, bound to the mutant m1-9 with a similar affinity as the more compliant GFP fusion protein bound to the parental mutant m1. Interestingly, this apparent gain in affinity was mostly due to a slower dissociation rate (k_{off}) in the case of m1-9.

A further remarkable rise in affinity was observed when the monovalent *Strep*-tag II was replaced by the Twin-*Strep*-tag in both fusion proteins (see Table 5). In this situation the mutant m1-9 (Strep-Tactin XT) revealed K_D values in the lower pM range, and a disadvantage of the cytochrome b_{562} fusion protein was no longer detectable. Like in the fluorescence titration experiments, these data illustrate the power of the avidity effect. For example, the complex half-life between the GFP fusion protein and the streptavidin mutants dramatically increased from 23 s, for the interaction between the monovalent *Strep*-tag II and m1, to 12.8 h in case of the interaction between the Twin-*Strep*-tag and m1-9. This was confirmed in a biolayer interferometry measurement, showing that complex formation between Strep-Tactin XT and the GFP Twin-*Strep*-tag fusion protein is kinetically extremely stable whereas the complex can be easily disintegrated under mild buffer conditions just by adding D-biotin as a competing ligand (Figure 7). Taken together, this wide range of complex stabilities, including ligand-triggered reversibility, which is now accessible with the *Strep*-tag system using our novel streptavidin mutants is ideal to cover a spectrum of applications, from affinity chromatography to the stable (and functional) surface adsorption of corresponding fusion proteins.

Discussion

The aim of this study was to identify streptavidin mutants that exhibit stronger affinity towards the artificial peptide ligand *Strep*-tag II than the previously developed mutant m1,[14] marketed as Strep-Tactin. An attempt to reoptimize the loop region 45–52 that had been engineered in m1 did not lead to a significant functional improvement but yielded the peculiar mutant m4001, which

Table 5 Real-time SPR affinity measurements between the immobilized streptavidin mutants and exemplary *Strep*-tag II fusion proteins (Strep: *Strep*-tag II; Twin: Twin-*Strep*-tag).

Fusion protein	Immobilized mutant	Protein density [ΔRU]	k_{on} [10^5 M^{-1} s^{-1}]	k_{off} [10^{-4} s^{-1}]	K_D [nM]
GFP-*Strep*	m1	325	1.00	300	300
		5567	1.90	250	130
	m1-9	170	1.50	47	32
		4350	1.70	38	23
GFP-Twin	m1	325	0.80	43	57
		5567	1.50	17	11
	m1-9	170	2.80	0.15	0.053
		4350	2.20	0.17	0.079
$Cytb_{562}$-*Strep*	m1	325	0.17	2900	16,700
		5567	0.14	2400	16,700
	m1-9	170	0.70	410	586
		4350	0.52	250	485
$Cytb_{562}$-Twin	m1	325	0.60	58	97
		5567	1.20	53	44
	m1-9	170	10.00	0.15	0.014
		4350	4.40	0.19	0.043

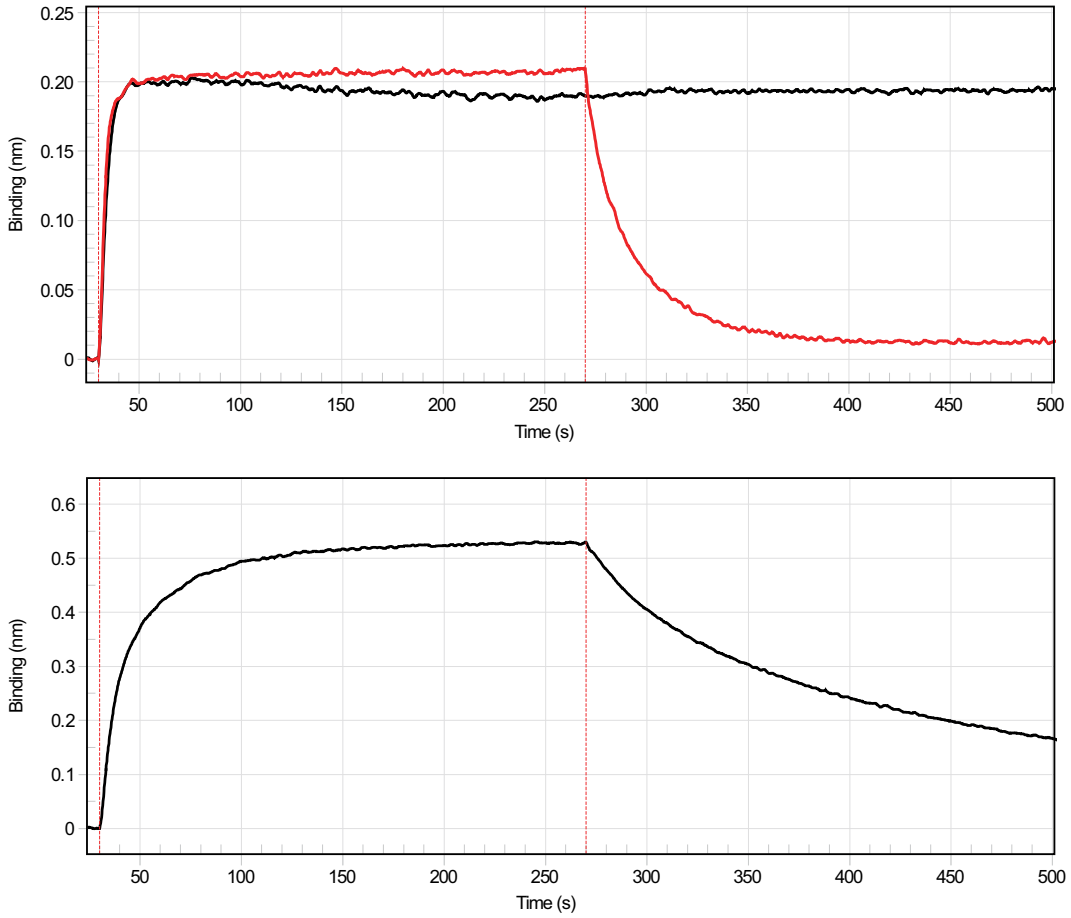

Figure 7. Interaction analysis between immobilized Strep-Tactin XT and the GFP Twin-*Strep*-tag fusion protein in comparison with the GFP *Strep*-tag II fusion protein via biolayer interferometry using the FortéBIO BLItz system. Top: The black curve shows the association between both binding partners followed by washing with buffer (starting at 270 s), which indicates extremely stable complex formation. The red curve shows the same protein association, however this time followed by washing with 50 mM D-biotin (dissolved in washing buffer), demonstrating that the complex can be readily dissociated in the presence of the small natural ligand of streptavidin as competitor. Bottom: The black curve shows the same association experiment with the monovalent GFP *Strep*-tag II fusion protein, this time followed by washing with buffer (starting at 270 s), indicating dissociation already in the absence of D-biotin.

carries a disulfide bridge at the base of the loop. This crosslink fixes the loop in an open conformation competent for the binding of the *Strep*-tag II, thus providing an alternative structural solution to the side chain substitutions at positions 44, 45 and 47 seen in the previously selected mutant m1.[21] In the next step, the loop 115–121 at the opposite side of the ligand pocket, which belongs to a different subunit of the streptavidin tetramer (see Figure 1), was chosen as target for further modification of Strep-Tactin. This was motivated by the observation of alternative side chain conformations of Trp120 as well as high crystallographic B factors, indicating enhanced structural flexibility in that region.[21] Random mutagenesis of this loop and subsequent screening of streptavidin mutants for binding of a reporter enzyme displaying the *Strep*-tag II revealed three sequence motifs with improved binding properties (cf. Table 3).

Motif 1 (represented by the mutant m1-9) is characterized by the occurrence of Gly at position 120, in combination with a bulky hydrophobic aromatic residue (Tyr or Phe) at position 121. This feature is accompanied by a larger variability at position 117, with some preference for the negatively charged residues Glu and Asp. Motif 2 (represented by the mutant m36) is dominated by positions 117 and 120, which are both occupied by bulky hydrophobic residues, mostly Phe and Tyr. When Phe or Tyr were predefined at position 117, as in the refined library #5, then Phe or Tyr also appeared as the preferred residues at position 120, together with a non-aromatic hydrophobic amino acid at position 121. Motif 3 (represented by the mutant m302) is characterized by the accidental deletion of the sequence positions 118 and 119. In this context, a Trp at the former position 120 (now 118) seemed

to be mandatory for enhanced binding of the *Strep*-tag II peptide. Trp occurred almost always at that position during subsequent screening of the refined library #6. When predefining this Trp residue, as in the further refined library #7, also a clear preference for Tyr at position 121 (now 119) emerged. This confirmed that the mutant m41, which produced the highest signal in the filter sandwich colony assay, indicated a close to optimal sequence motif already in the initial library #3 (see Table 2). Preferences at position 117 were less pronounced while His, Gln, Glu and Ala led to the strongest signals when finally screening the library #7.

To elucidate the structural basis for the improved binding properties of representative streptavidin mutants covering these three motifs, we crystallized the complexes of m1-9, m36 and m302 with the *Strep*-tag II peptide. As expected, the gross structure of the streptavidin tetramer was retained in all cases and the peptide ligand was always bound at the same position at the open end of the β-barrel – like in the crystal structure of the mutant m4001 carrying the engineered disulfide bridge described further above. While the detailed structural arrangements within the ligand pocket differed considerably between the mutants with an engineered 115–121 loop, all three motifs appeared to create more space in the pocket, allowing better accommodation of the *Strep*-tag II peptide, especially with regard to the positioning of the peptide residue Phe8. Notably, Phe was a clearly preferred amino acid at position 8 during the initial selection of the *Strep*-tag sequence in the context of wtSA as interaction partner.[10]

Remarkably, in motif 1 the bulky Trp120 was replaced by Gly, which lacks any side chain. Apparently, this radical increase in space is counterbalanced by the exchange of Lys121 by Tyr (or Phe) at the neighboring position, which also provides better hydrophobic contacts with the peptide residue Phe8. The preference for a negatively charged residue at position 117 is explained by the formation of a second salt bridge with Lys10 of the peptide. In motif 2, the new pair of residues Phe120 and Met121 has similar space requirements as the original residues Trp and Lys at these positions (cf. Table 3). However, in this case the backbone conformation of the loop 115–121 is strongly altered due to the occurrence of Tyr instead of Ala at position 117; as a consequence, the unmutated neighboring residue Glu116 takes over the role of Glu117 from motif 1 (as seen in the mutant m1-9) by forming the salt bridge with Lys10 of the *Strep*-tag II. In motif 3, the unexpected deletion of residues 118 and 119, together with a totally new conformation of the shortened loop, reveals another, more drastic solution how to provide increased space to the binding pocket. In this situation, the bulky hydrophobic side chain of Trp120 (now sequence position 118) was conserved in all mutants emerging from the screen for improved binding of the *Strep*-tag II (see library #6 in Table 3), together with a strongly preferred Tyr at position 121 (now 119, dominating the hits from library #7).

Taken together, our combined mutational and crystallographic studies illustrate the many structural solutions and the large conformational space offered by the two dominant loops that shape the entrance to the ligand pocket of the streptavidin β-barrel. In some aspects this resembles another widespread family of binding proteins that rely on a β-barrel fold, the lipocalins.[24] In this case, the combinatorial reshaping of four structurally variable loops which together form the entrance to the ligand pocket has led to a novel class of binding proteins, called Anticalins, that offer diverse ligand specificities towards small molecules, peptides and proteins.[25]

To finally choose a suitable streptavidin mutant with improved binding properties for practical applications, not only the affinity for the *Strep*-tag II peptide ligand has to be taken into account but also other factors come into play. One relevant feature is a high stability of the mutated streptavidin to enable the preparation of robust affinity columns that can withstand stringent cleaning procedures. Another feature concerns the functional binding activity for a small biotin derivative, which must be strong enough to effect sharp elution of a bound *Strep*-tag II fusion protein but also should be reversible, thus allowing the repeated regeneration of the affinity column by washing with buffer.[13] As a result of such experimental tests (not shown here), the mutant m1-9, marketed as Strep-Tactin XT, emerged as the candidate with the most advantageous overall attributes. Applied in an immobilized form or labelled in different varieties, Strep-Tactin XT considerably expands the *Strep*-tag tool box, in particular if combined with the Twin-*Strep*-tag as affinity partner. In this way, important new applications have become possible, including protein immobilization in sensor chip technology, cell separation or protein purification under denaturing conditions.

Recently, the *Strep*-tag system has attracted particular popularity in the field of SARS-CoV-2 research, both to support basic studies and to prepare for an effective vaccine against viral infections. Prominent examples include the FluoroSpot method for testing the human B cell memory response,[26] the application of Strep-Tactin XT in the elucidation of a SARS-CoV-2 protein interaction map[27] and use of *Strep*-tag affinity purification to investigate the structural basis for the recognition of human ACE2 by SARS-CoV-2.[28] Another interesting application relates to the use of the *Strep*-tag II in the design of antigen receptors for T-cell immunotherapy.[29] Our expanded *Strep*-tag tool box shows promise to

boost research also in other topical areas of virology, cell biology, bacteriology and protein science.

Materials & Methods

Targeted randomization of streptavidin and molecular cloning procedures

The construction of mutated streptavidin gene libraries was based on pASK-IBA2-SAm1, a derivative of pASK75-Sap,[14] which carries the coding region for the mutant 1 (*Strep*-Tactin) instead of wtSA. The plasmid libraries #1 and #2 with the randomized positions in the amino acid sequence stretch 44–52 were prepared by PCR amplification of the larger part of the coding region from pASK-IBA2-SAm1 with *Pfu* DNA polymerase (Thermo Fisher Scientific, Waltham, MA) using the 3′-phosphorothioate protected[30] forward primers 5′-TCG TGA CCG CGG GTG CAG ACG GAG CTC TGA CCG GTA CCT ACN N(C/G)N N(G/T)G CGC GTG GCA ACG CCG AGN N(C/G)C GCT ACG TCC TGA CCG GTC GTT and 5′-CTG ACC GGT ACC TAC G(G/C)T TGC NN(G/C) NN(G/T) GGC AAC GCC GAG TGC CGC TAC GTC CTG A, respectively, each together with the reverse primer 5′-AGT AGC GGT AAA CGG CAG A (IBA, Göttingen, Germany). The 32-fold degenerate codons in the forward primer, which cover the mutated stretch, were chosen to encode all 20 amino acids but only one of the three stop codons. The resulting PCR product was cut with the restriction enzymes *Kpn*I and *Hin*dIII and ligated with the likewise cut vector fragment of pASK-IBA2-SAm1. Prior to the filter sandwich colony screening assay, *E. coli* TOP10 cells (Thermo Fisher Scientific) were transformed with the ligation mixture using the calcium chloride method.[31]

Libraries #3 to #7 harboring randomized positions in the amino acid sequence region 117–121 were prepared by PCR amplification of the entire plasmid template using *Pfu* Ultra polymerase (Agilent Technologies, Santa Clara, CA) and oligodeoxynucleotides priming into opposite directions, which were positioned within the mutagenized sequence stretch with adjacent (phosphorylated) 5′-ends. For example, the 5′-nucleotide of the forward primer represented the first nucleotide of the codon for amino acid 119 while the 5′-nucleotide of the reverse primer corresponded to the third nucleotide of the codon for amino acid 118 on the complementary DNA strand. Together with the high processivity of *Pfu* Ultra polymerase, this strategy involves just a single intramolecular ligation of the PCR product to yield a functional circular plasmid DNA and offers an advantage over a less efficient conventional (bimolecular) ligation reaction. Furthermore, there was no need to introduce suitable restriction sites, and the potentially inefficient cleavage close to the end of a PCR product was circumvented. As a result of the intramolecular blunt end ligation a highly diverse plasmid library was obtained with randomized positions on both sides of the ligation site. On the other hand, this random mutagenesis strategy also explains the occurrence of deletion mutants as described in the text in case of oligodeoxynucleotide primers that were contaminated with 5′-shortened DNA synthesis products.

The template for the libraries #3 and #5 to #7 was pASK-IBA2-SAm1 whereas pASK-IBA2-SAm4001, which carries the optimized sequence of the amino acid stretch 44–52 from the screening of libraries #1 and #2 (see text), was used as template for the library #4. The resulting PCR products were purified by agarose gel electrophoresis and ligated, followed by transformation of *E. coli* TOP10 cells via electroporation with a Micro Pulser (Bio-Rad Laboratories, Hercules, CA) at 2.5 kV using 0.2 cm cuvettes and the manufacturer's standard program Ec2. The forward/reverse primer pair 5′-GCC NN(G/C) NN (G/T) TCC ACG CTG GTC GGC CA/5′-GTT (A/C) NN CTC GGT GGT GCC GGA GGT was used for libraries #3 and #4 and the forward/reverse primer pairs 5′-GCC NN(G/C) NN(G/T) TCC ACG CTG GTC GGC CA/5′-GTT A(A/T)A CTC GGT GGT GCC GGA GGT, 5′-N(G/C)N N(G/T)T CCA CGC TGG TCG GCC AC/5′-N(A/C)N NCT CGG TGG TGC CGG AGG T and 5′-GGN N(G/T)T CCA CGC TGG TCG GCC AC/5′-A(C/A)N NCT CGG TGG TGC CGG AGG T were used for libraries #5, #6 and #7, respectively.

Filter sandwich colony screening assay

The plasmid libraries from above were subjected to the filter sandwich colony screening assay essentially as described before.[14,32] To this end, the freshly transformed *E. coli* cells were plated onto nitrocellulose acetate membranes (type OE66, 110 mm diameter; Whatman, Dassel, Germany) placed on top of an Immobilon-P capture membrane (Millipore, Schwalbach am Taunus, Germany) which had been coated with anti-streptavidin immunoglobulin (Sigma-Aldrich, St. Louis, MO). LB agar medium[31] containing 100 mg/ml ampicillin and supplemented with 0.2 mg/ml anhydrotetracycline (aTc)[33] was used for induction of streptavidin gene expression and protein secretion during colony growth. Subsequently, the capture membrane was separated, washed and immersed in 10 ml phosphate-buffered saline (PBS; 4 mM KH_2PO_4, 16 mM Na_2HPO_4, 115 mM NaCl) containing 0.1 % v/v Tween and 2 μg/ml PhoA/Strep-tag II fusion enzyme[14] as reporter reagent. Incubation was performed for 1 h at room temperature, followed by washing twice with PBS-Tween and twice with PBS. The signals were then developed for 1–2 h in the presence of 10 ml AP buffer (100 mM Tris/HCl pH 8.8, 100 mM NaCl, 5 mM $MgCl_2$) with the addition of 30 μl BCIP

(50 mg/ml 5-bromo-4-chloro-3-indolyl phosphate 4-toluidine salt in dimethylformamide) and 5 μl NBT (75 mg/ml nitro blue tetrazolium in 70 % v/v dimethylformamide). Finally, colonies on the upper (support) membrane corresponding to colored spots on this second membrane were identified and propagated.

Bacterial expression of streptavidin mutants and affinity analyses

The *Sac*II/*Hin*dIII fragment was excised from each mutated pASK-IBA2-SAm1 plasmid and used to replace the equivalent coding region for wtSA on the T7 promoter vector pSA1.[13] In case of the mutant m1-9, which was originally selected from the library #4 based on m4001 as the mutant "m9", the C-terminal coding region was subcloned on pSA1-m1, thus grafting the modified loop 115–121 into the context of the 44–52 loop region of the mutant m1 to allow for better comparison with the other loop motifs described in the text. The streptavidin mutants were then expressed as cytoplasmic inclusion bodies, solubilized, renatured and purified by fractionated ammonium sulfate precipitation as previously described. The purity of the isolated streptavidin mutants was typically > 90 % as determined with a 2100 Bioanalyzer (Agilent). Protein concentrations were measured via the absorbance at 280 nm using calculated extinction coefficients.[34]

Ligand-binding equilibria were quantified by means of fluorescence titration according to a published procedure.[14] Each purified streptavidin mutant at a concentration of 1 μM in 2 mL 100 mM Tris/HCl pH 8.0 was titrated at 25 °C with aliquots of the synthetic peptide solution (0.1 mM 2-Abz-SAWSHPQFEK-NH_2; GenScript, Piscataway, NJ) up to a final volume of 40 μl and the Tyr/Trp fluorescence intensity was measured in an LS 50 instrument (Perkin-Elmer, Norwalk, CT). For kinetic interaction studies, the streptavidin mutants were covalently immobilized onto a CM5 sensor chip using standard amine coupling chemistry and the binding/dissociation kinetics of several test proteins, in particular GFP[17] and cytochrome b_{562},[13] fused with a C-terminal *Strep*-tag II or Twin-*Strep*-tag[12] were measured in the presence of 10 mM HEPES/NaOH pH 7.4 at 25 °C by real-time surface plasmon resonance (SPR) analysis on a Biacore 2000 instrument operated by Biaffin (Kassel, Germany). To analyze the kinetics of the interaction between the streptavidin mutant m1-9 and GFP fused with the Twin-*Strep*-tag or *Strep*-tag II, m1-9 was coupled to Amine Reactive Second-Generation (AR2G) Biosensors (Sartorius BioAnalytical Instruments, New York, NY). To this end, sensors were activated with EDC/NHS for 10 min and then incubated for 10 min with 45 μg/ml Strep-Tactin XT in 10 mM Na-acetate pH 5, followed by blocking with 1 M ethanolamine/HCl pH 8.5 for 10 min. After equilibration of the sensors in washing buffer (100 mM Tris/HCl, 150 mM NaCl, 1 mM EDTA, pH 8.0), the association and dissociation of the GFP, applied at 33 μg/ml in washing buffer (which was optionally supplemented with 50 mM D-biotin) was analyzed using a BLItz system (Sartorius BioAnalytical Instruments).

Preparation of complexes between streptavidin mutants and *Strep*-tag peptides

The purified streptavidin mutants were dialyzed against 10 mM Tris/HCl pH 8.0 and concentrated using 10 kDa MWCO Vivaspin 20 ultrafiltration units (Sartorius, Göttingen, Germany): 18 mg/ml for m4001, 8 mg/ml for m302, 17 mg/ml for m36, 13 mg/ml for m1-9 (single), 11 mg/ml for m1-9 (twin) and 33 mg/ml for m1 (twin). Prior to complex formation and crystallization, all proteins were centrifuged and subsequently filtrated through an Amicon Ultrafree centrifugal filter (0.45 μm; Merck Millipore, Billerica, MA) to remove any aggregates. Then, each protein was mixed with the respective peptide (both from GenScript) dissolved in water as mentioned in the text, i.e. *Strep*-tag II (dubbed "single") or Twin-*Strep*-tag (dubbed "twin"). Molar ratios were 1:2 for m4001/single, m302/single, m1-9/single and 1:3 for m36/single, m1-9/twin, m1/twin. The solutions of the complex preparations m36/single and m1/twin appeared cloudy after mixing and, thus, were filtered again as above.

Crystallization of streptavidin/peptide complexes

In total 6 complexes between the purified streptavidin mutants and the *Strep*-tag II (2-Abz-SAWSHPQFEK-NH_2) or the Twin-*Strep*-tag (2-Abz-SAWSHPQFEKGGGSGGGSGGGSAWSHPQFEK-NH_2) were crystallized (Table 2). Crystals for the combinations m4001/single, m302/single and m1-9/single were obtained with the sitting drop vapor diffusion method. The drops were prepared from 250 nl protein/peptide solution (see above) and 250 nl reservoir solution using an in house precipitant screen at 20 °C (for crystallization conditions, see Table 2). For reasons of molecular symmetry discussed in the text, conditions were searched for complexes of the Twin-*Strep*-tag yielding crystals with one tetramer of the streptavidin mutant in the asymmetric unit, similar to a T7-tagged streptavidin that had been crystallized in the presence of 25 % (w/v) $(NH_4)_2SO_4$, 0.1 M Na-acetate pH 4.5[35] (PDB ID: 2BC3). The complexes of the streptavidin mutants m1 and m1-9 with the Twin-*Strep*-tag, and also the one of m36/single, were crystallized using the hanging drop vapor diffusion method with drops consisting of 1 μl protein/peptide solution and 1 μl reservoir solution in the presence of $(NH_4)_2SO_4$ as precipitant (cf. Table 2). The crystals were harvested, transferred into the precipitant buffer sup-

plemented with 30 % (v/v) glycerol (m36/single, m1-9/twin, m1/twin), 25 % (v/v) PEG200 (m302/single, m1-9/single) or 30 % (v/v) PEG200 (m4001/single), and immediately frozen in liquid nitrogen prior to transfer to the X-ray source.

X-ray diffraction data collection and structure solution

Single-wavelength synchroton data sets were collected at 100 K from crystals of the streptavidin/peptide complexes at beamlines 14.1 and 14.2 of the Helmholtz-Zentrum Berlin, Germany.[36] The diffraction data, with resolutions from 1.5 to 2.2 Å (see Table 2), were processed with MOSFLM and scaled with SCALA.[37] Molecular replacement was performed with MrBUMP and Phaser[37] using the crystal structure of the T7-tagged streptavidin[35] (PDB ID: 2BC3) as search structure for the complexes m4001/single and m302/single and the one of the complex between wtSA and the *Strep*-tag peptide[11] (PDB ID: 1RST) for m36/single, m1-9/single, m1-9/twin and m1/twin. The protein models were manually adjusted with Coot[38], water molecules were added with ARP/wARP[37] and structural refinement was performed with Refmac5[37], including model correction via the PDB_REDO server[39]. The final structural models were validated with PROVE,[40] ERRAT,[41] Verify3D,[42] PROCHECK,[43] WHAT_CHECK[44] and by using the MolProbity server.[45] The crystallographic data and refinement statistics are reported in Table 2. Secondary structure elements were assigned with DSSP[46] and crystal contact sites were analyzed with PISA.[47] Graphics were prepared with PyMOL.[48] The atomic coordinates and structure factors of the refined streptavidin/peptide complexes have been deposited at the Protein Data Bank (PDB; Research Collaboratory for Structural Bioinformatics, Rutgers University, New Brunswick, NJ), under accession codes 6QW4 (m4001/single), 6QSY (m302/single), 6TIP (m36/single), 6QBB (m1-9/single), 6SOS (m1-9/twin), and 6SOK (m1/twin). Note that the structure of the complex m36/single contains two monomers in the asymmetric unit, and each monomer is part of a neighboring tetramer in the crystal lattice; while one monomer (chain A) is well defined in the electron density, the density of the second monomer (chain B) is inferior and only its Cα coordinates were deposited. When applying crystallographic symmetry ($P4_22$), chain A gives rise to a fully defined (biological) tetramer including all side chains.

Accession Numbers

PDB: 6QW4, 6QSY, 6TIP, 6QBB, 6SOS, 6SOK

CRediT authorship contribution statement

Thomas G.M. Schmidt: Conceptualization, Supervision, Writing - original draft, Writing - review & editing. **Andreas Eichinger:** Investigation, Visualization, Writing - original draft, Writing - review & editing. **Markus Schneider:** Investigation, Writing - review & editing. **Lidia Bonet:** Investigation, Writing - review & editing. **Uwe Carl:** Resources, Writing - review & editing. **Dennis Karthaus:** Investigation, Writing - review & editing. **Ina Theobald:** Investigation, Writing - review & editing. **Arne Skerra:** Conceptualization, Supervision, Writing - original draft, Writing - review & editing.

Acknowledgements

The authors wish to thank Lilia Batz (IBA) and Stefan Achatz (TUM) for excellent technical support and Karine Sparta and Dr. Manfred S. Weiss for assistance at BESSY beamlines 14.1 and 14.2, Helmholtz-Zentrum Berlin, Germany. This work was financially supported by the Helmholtz-Zentrum Berlin, Germany. *Strep*-tag®, Twin-*Strep*-tag® and Strep-Tactin® are registered trademarks of IBA GmbH, Göttingen, Germany.

Declaration of Competing Interest

T.S. is a shareholder of IBA GmbH. The other authors declare that they have no known competing financial interests or personal relationships that could have appeared to influence the work reported in this paper.

Received 24 November 2020;
Accepted 18 February 2021;
Available online 24 February 2021

Keywords:
affinity system;
avidity effect;
peptide ligand;
protein-peptide complex;
streptavidin

References

1. Arnau, J., Lauritzen, C., Petersen, G.E., Pedersen, J., (2006). Current strategies for the use of affinity tags and tag removal for the purification of recombinant proteins. *Protein Expr. Purif.*, **48**, 1–13.
2. Kosobokova, E.N., Skrypnik, K.A., Kosorukov, V.S., (2016). Overview of fusion tags for recombinant proteins. *Biochemistry (Mosc).*, **81**, 187–200.
3. Li, Y., (2010). Commonly used tag combinations for tandem affinity purification. *Biotechnol. Appl. Biochem.*, **55**, 73–83.
4. Mahmoodi, S., Pourhassan-Moghaddam, M., Wood, D.W., Majdi, H., Zarghami, N., (2019). Current affinity approaches for purification of recombinant proteins. *Cogent. Biol.*, **5**, 1665406.

5. Saraswat, M., Musante, L., Ravida, A., Shortt, B., Byrne, B., Holthofer, H., (2013). Preparative purification of recombinant proteins: current status and future trends. *Biomed. Res. Int.*, **2013**, 312709.
6. Waugh, D.S., (2005). Making the most of affinity tags. *Trends Biotechnol.*, **23**, 316–320.
7. Kimple, M.E., Sondek, J., (2002). Affinity tag for protein purification and detection based on the disulfide-linked complex of InaD and NorpA. *Biotechniques*, **33**, 578–590.
8. Young, C.L., Britton, Z.T., Robinson, A.S., (2012). Recombinant protein expression and purification: a comprehensive review of affinity tags and microbial applications. *Biotechnol. J.*, **7**, 620–634.
9. Diamandis, E.P., Christopoulos, T.K., (1991). The biotin-(strept)avidin system: principles and applications in biotechnology. *Clin. Chem.*, **37**, 625–636.
10. Schmidt, T.G., Skerra, A., (1993). The random peptide library-assisted engineering of a C-terminal affinity peptide, useful for the detection and purification of a functional Ig Fv fragment. *Protein Eng.*, **6**, 109–122.
11. Schmidt, T.G., Koepke, J., Frank, R., Skerra, A., (1996). Molecular interaction between the *Strep*-tag affinity peptide and its cognate target, streptavidin. *J. Mol. Biol.*, **255**, 753–766.
12. Schmidt, T.G., Batz, L., Bonet, L., Carl, U., Holzapfel, G., Kiem, K., et al., (2013). Development of the Twin-Strep-tag® and its application for purification of recombinant proteins from cell culture supernatants. *Protein Expr. Purif.*, **92**, 54–61.
13. Schmidt, T.G., Skerra, A., (1994). One-step affinity purification of bacterially produced proteins by means of the “Strep tag” and immobilized recombinant core streptavidin. *J. Chromatogr. A*, **676**, 337–345.
14. Voss, S., Skerra, A., (1997). Mutagenesis of a flexible loop in streptavidin leads to higher affinity for the *Strep*-tag II peptide and improved performance in recombinant protein purification. *Protein Eng.*, **10**, 975–982.
15. Schmidt, T.G., Skerra, A., (2007). The *Strep*-tag system for one-step purification and high-affinity detection or capturing of proteins. *Nat. Protoc.*, **2**, 1528–1535.
16. Skerra, A., Schmidt, T.G., (2000). Use of the *Strep*-tag and streptavidin for detection and purification of recombinant proteins. *Methods Enzymol.*, **326**, 271–304.
17. Skerra, A., Schmidt, T.G., (1999). Applications of a peptide ligand for streptavidin: the *Strep*-tag. *Biomol. Eng.*, **16**, 79–86.
18. Schmidt, T., Skerra, A., (2015). The *Strep*-tag system for one-step affinity purification of proteins from mammalian cell culture. *Methods Mol. Biol.*, **1286**, 83–95.
19. Yeliseev, A., Zoubak, L., Schmidt, T.G.M., (2017). Application of Strep-Tactin XT for affinity purification of Twin-Strep-tagged CB_2, a G protein-coupled cannabinoid receptor. *Protein Expr. Purif.*, **131**, 109–118.
20. Weber, P.C., Ohlendorf, D.H., Wendoloski, J.J., Salemme, F.R., (1989). Structural origins of high-affinity biotin binding to streptavidin. *Science*, **243**, 85–88.
21. Korndörfer, I.P., Skerra, A., (2002). Improved affinity of engineered streptavidin for the *Strep*-tag II peptide is due to a fixed open conformation of the lid-like loop at the binding site. *Protein Sci.*, **11**, 883–893.
22. Meir, A., Helppolainen, S.H., Podoly, E., Nordlund, H.R., Hytönen, V.P., Määttä, J.A., et al., (2009). Crystal structure of rhizavidin: insights into the enigmatic high-affinity interaction of an innate biotin-binding protein dimer. *J. Mol. Biol.*, **386**, 379–390.
23. Chilkoti, A., Tan, P.H., Stayton, P.S., (1995). Site-directed mutagenesis studies of the high-affinity streptavidin-biotin complex: contributions of tryptophan residues 79, 108, and 120. *Proc. Natl. Acad. Sci. USA*, **92**, 1754–1758.
24. Skerra, A., (2000). Lipocalins as a scaffold. *Biochim. Biophys. Acta*, **1482**, 337–350.
25. Richter, A., Eggenstein, E., Skerra, A., (2014). Anticalins: exploiting a non-Ig scaffold with hypervariable loops for the engineering of binding proteins. *FEBS Lett.*, **588**, 213–218.
26. Varnaitė, R., García, M., Glans, H., Maleki, K.T., Sandberg, J.T., Tynell, J., et al., (2020). Expansion of SARS-CoV-2-specific antibody-secreting cells and generation of neutralizing antibodies in hospitalized COVID-19 patients. *J. Immunol.*, **205**, 2437–2446.
27. Gordon, D.E., Jang, G.M., Bouhaddou, M., Xu, J., Obernier, K., O’Meara, M.J., et al., (2020). A SARS-CoV-2 protein interaction map reveals targets for drug repurposing. *Nature*, **583**, 459–468.
28. Yan, R., Zhang, Y., Li, Y., Xia, L., Guo, Y., Zhou, Q., (2020). Structural basis for the recognition of SARS-CoV-2 by full-length human ACE2. *Science*, **367**, 1444–1448.
29. Liu, L., Sommermeyer, D., Cabanov, A., Kosasih, P., Hill, T., Riddell, S.R., (2016). Inclusion of *Strep*-tag II in design of antigen receptors for T-cell immunotherapy. *Nat. Biotechnol.*, **34**, 430–434.
30. Skerra, A., (1992). Phosphorothioate primers improve the amplification of DNA sequences by DNA polymerases with proofreading activity. *Nucleic Acids Res.*, **20**, 3551–3554.
31. Sambrook, J., Fritsch, E.F., Maniatis, T., (1989). Molecular Cloning: A Laboratory Manual. Cold Spring Harbor Laboratory Press, Cold Spring Harbor, New York.
32. Skerra, A., Dreher, M.L., Winter, G., (1991). Filter screening of antibody Fab fragments secreted from individual bacterial colonies: specific detection of antigen binding with a two-membrane system. *Anal. Biochem.*, **196**, 151–155.
33. Skerra, A., (1994). Use of the tetracycline promoter for the tightly regulated production of a murine antibody fragment in *Escherichia coli*. *Gene*, **151**, 131–135.
34. Gill, S.C., von Hippel, P.H., (1989). Calculation of protein extinction coefficients from amino acid sequence data. *Anal. Biochem.*, **182**, 319–326.
35. Le Trong, I., Humbert, N., Ward, T.R., Stenkamp, R.E., (2006). Crystallographic analysis of a full-length streptavidin with its C-terminal polypeptide bound in the biotin binding site. *J. Mol. Biol.*, **356**, 738–745.
36. Mueller, U., Darowski, N., Fuchs, M.R., Förster, R., Hellmig, M., Paithankar, K.S., et al., (2012). Facilities for macromolecular crystallography at the Helmholtz-Zentrum Berlin. *J. Synchrotron Radiat.*, **19**, 442–449.
37. CCP4, (1994). The CCP4 suite: programs for protein crystallography. *Acta Crystallogr. D Biol. Crystallogr.*, **50**, 760–763.
38. Emsley, P., Cowtan, K., (2004). Coot: model-building tools for molecular graphics. *Acta Crystallogr. D Biol. Crystallogr.*, **60**, 2126–2132.
39. Joosten, R.P., Long, F., Murshudov, G.N., Perrakis, A., (2014). The PDB_REDO server for macromolecular structure model optimization. *IUCrJ.*, **1**, 213–220.
40. Pontius, J., Richelle, J., Wodak, S.J., (1996). Deviations from standard atomic volumes as a quality measure for protein crystal structures. *J. Mol. Biol.*, **264**, 121–136.

41. Colovos, C., Yeates, T.O., (1993). Verification of protein structures: patterns of nonbonded atomic interactions. *Protein Sci.*, **2**, 1511–1519.
42. Luthy, R., Bowie, J.U., Eisenberg, D., (1992). Assessment of protein models with three-dimensional profiles. *Nature*, **356**, 83–85.
43. Laskowski, R.A., MacArthur, M.W., Mos, D.S., Thornton, J. M., (1993). PROCHECK: a program to check the stereochemical quality of protein structures. *J. Appl. Cryst.*, **26**, 283–291.
44. Hooft, R.W., Vriend, G., Sander, C., Abola, E.E., (1996). Errors in protein structures. *Nature*, **381**, 272.
45. Chen, V.B., Arendall 3rd, W.B., Headd, J.J., Keedy, D.A., Immormino, R.M., Kapral, G.J., et al., (2010). MolProbity: all-atom structure validation for macromolecular crystallography. *Acta Crystallogr. D Biol. Crystallogr.*, **66**, 12–21.
46. Kabsch, W., Sander, C., (1983). Dictionary of protein secondary structure: pattern recognition of hydrogen-bonded and geometrical features. *Biopolymers*, **22**, 2577–2637.
47. Krissinel, E., Henrick, K., (2007). Inference of macromolecular assemblies from crystalline state. *J. Mol. Biol.*, **372**, 774–797.
48. DeLano, W.L., (2002). The PyMOL Molecular Graphics System. DeLano Scientific, San Carlos, CA, USA.
49. Arndt, U.W., Crowther, R.A., Mallett, J.F.W., (1968). A computer-linked cathode-ray tube microdensitometer for X-ray crystallography. *J. Phys. E: Sci. Instrum.*, **1**, 510–516.
50. Wilson, A., (1950). Largest likely values for the reliability index. *Acta Cryst.*, **3**, 397–398.
51. Brunger, A.T., (1997). Free R value: cross-validation in crystallography. *Methods Enzymol.*, **277**, 366–396.